Crystal Structures of Fsa2 and Phm7 Catalyzing [4 + 2] Cycloaddition Reactions with Reverse Stereoselectivities in Equisetin and Phomasetin Biosynthesis

Changbiao Chi,[1,‡] Zhengdong Wang,[1,‡] Tan Liu,[1] Zhongyi Zhang,[1] Huan Zhou,[2] Annan Li,[1] Hongwei Jin,[1] Hongli Jia,[1] Fuling Yin,[1] Donghui Yang,[1] and Ming Ma[1,*]

[1]State Key Laboratory of Natural and Biomimetic Drugs, School of Pharmaceutical Sciences, Peking University, 38 Xueyuan Road, Haidian District, Beijing 100191, China

[2]Shanghai Synchrotron Radiation Facility, Shanghai Advanced Research Institute, Chinese Academy of Sciences, 239 Zhangheng Road, Pudong District, Shanghai 201204, China

‡These authors contributed equally
*To whom correspondence should be addressed: Ming Ma, E-mail: mma@bjmu.edu.cn

Table of Contents

The optimized gene sequence of *fsa2* and *phm7* for expression in *E. coli*

The optimized gene sequence of *fsa2*:

ATGTCCAACGTGACCGTATCCGCATTCACGGTCGATAAGAGCATCAGCGAGGAGCATGTCCTGCCTAG

CAGCTTCATTCCGGGTAGCGGTAACATCTTCCCAAAGTTCACCTCCGCAATCCCAAAGACGGCTTGGG

AGCTGTGGTACTTTGACGGTATCAGCAAAGACGACAAAAGCTCCATCGTCATCGGTGTGACCCGTAAC

GCGGAGGGTCTGAAACATGGTGGTTTCAAAGTGCAGGTCTTCGTGATCTGGGCAGACGAACGTACGT

GGCACCGTGACCTGTTCTTCCCGGAATCCGTGGTGTCTATCAACGAATCCGGTGTAACCGACGGTATTT

GGAAAGACGCTACGAGCAACAGCTCTATCAGCTTCAGCTGCGCTGGTGATCTGTCCAAAGCATCCCTG

GTGTTCGACGTGCCGGGCGTGGTACAGGGTGACATGCACCTGGAAGCTCTGCCAGGTGATACTGGTCT

GGATACTGACGCACGTCTGGGTCCGTCTGTTTACTATGTTCGTCCGATCGGTCGTGCTTCTGTAAAAGC

CCAGCTGTCTCTGTACAGCTCCGACGCTACTGCGGCGGAACAATTTTCCCTGGGTACTTCCGCGAATG

GTGGTATGGATCGTGTTTGGTCCCCGCTGTCTTGGCCGCAAGTAATGACTGAATCTTACTACCTGCGCA

CTCAGGTTGGTCCGTACGCCATGCAAATCATGCGTATTTTTCCGCCGGCCGGTTCTGAAGATCAGCCGT

CTACCATGGCGCGTCTGTACCGCGAAGGCCAGCTGGTTTGTGTTGCGCAGCACGTTGTAACTCGCGAA

GATGCGCTGATGACCCACGATTCTCTGATTCTGTCTAAACAGGATAACTCCGACTCTGAAGACGTTGTT

ACCGGCGGCTATCGTGATAAAAACACCGGCTATACCGTTGAATTTGTTGAAAAAGGCAACGAGGGCCA

GCGTTGGAAATTTCAGGTACGCCACGAACGCATCATTTGGAACACCCCGACCTCTCGCCCTGGCCCGG

ATGCCACCGGCAATACCGGCTTCGTTGAAGTTCTGTGCGGCGGCACCATTGGCGAATCTTATGAAGGC

GTTGGCACTGGCGGCCAGTGTGAACTGTCTAA

The optimized gene sequence of *phm7*:

ATGAGCGAACCGACCTCAAGCAGTAGTCTGGATATTACCAGTAATTGCATTATTGAAACCCCGCTGCAG

CCGAGCGATTTTCTGCCTAAAAGTGCCAATCTGTTTCCGAAATTTCCGGAACGCATTAGCGTTGATAGC

TGGGAACTGTGGGAATTTGATACCTTTGATACCAATGGTAGTGTTGCATTTGGTTGCAGTCTGTATCGT

GATGCACGTGGCGTTGAACAGGGCGGTTTTCATGCCGAAGTTAATGCCCTGTGGCCGGATGGTACCCA

TTGGGGTGAAACCCTGTATTTTGCCGTTAGCGAAGTTGTTGAAAATAGTGATGGTACCACCGGTGGCA

AATGGCTGAGTAAAGATGGTGGTAGCATTACCTTTCATATTGCCAGTGATTATACCGCCGCCGCACTGG

ATTTTAATGTGCCGGGTAAAGTTAGCGGTACCATGGAACTGCGCAATCATGCCAATGTTAGTCCGACCA

GTAATCTGCCGGCAAGTGATGCCGAAGCACAGTTATGTCCGGGCGTGTATTATACCTTTCCGATGGGTC

CGGTGGCAACCTCAGTGACAGCAACATTTTCAAGCGTTGGCGCCAATGGCGAAAGCCGTGAACTGTT

TATTAGTAGCGGCTATGGCGGTATGGTTCGTGGCTGGTCAGCCAGACCTTGGCCTACATTCATGAATGA

TGCCTATTATGTTGTTGCCCAGGTGGGCCCGTATATGCTGCAAATTCTGCGCACCCTGGGCAGTGTGTT

TGTGCAACATAAACCGTTTGCAGTTGCCCGCCTGTATCTGGATGGCTCACTGGTTAGTGCAGCCAATAC

CGTTGTGGGCGATGAACTGACCGCACATGCAGATGATGTTAAAGGTGACGCAGTTCGCCTGACCAAA

GTGCAGCCTGATGAAAAAAGCCAGGGCCTGAGCGGTAAATTTCGTGATGGCAATGTTGGCTATGTGCT

GGAATTTGCAAAAAAGGATAGTGAACATGGTTGGACCTTTCAGATTAGCCATAAACGTGCAGTTTGGA

GTGAACCGACCAGTGCCCCTGGTCCTGATGGTACAGGTAAAAGTGGCTGGATTGAAGCCATTAGCGGC

GGTGCAAAAGGCGAAAATTATGAAGGTCATGGCTTTGGTGGTCAGCTGCAGATTCCGGTGCCGTAA

Table S1. Plasmids used in this study

Plasmids	Description	Sources
pMM4005	Modified pET28b(+) containing *fsa2* gene for protein production	This work
pMM4006	Modified pET28b(+) containing *phm7* gene for protein production	This work

Table S2. The X-ray data collection and refinements statistics

	Fsa2	**Phm7**
Data collection		
Wavelength (Å)	1.54056	1.54056
Space group	$P2_12_12_1$	$P2_1$
Unit cell		
a, *b*, *c* (Å)	85.0, 82.4, 48.2	91.2, 150.5, 100.0
α, *β*, *γ* (°)	90.0, 90.0, 90.0	90.0, 96.9, 90.0
Resolution range (Å)	13.59–2.00	13.42–2.00
	(2.07–2.00)	(2.07–2.00)
Unique reflections	23,436 (2,349)	179,300 (17,930)
R_{merge}[a]	0.09 (0.363)	0.130 (0.423)
$I/\sigma I$	26.86 (7.15)	11.33 (3.43)
Completeness (%)	99.3 (99.3)	99.5 (99.9)
Average redundancy	12.6 (13.1)	6.7 (6.9)
Structure refinements		
Resolution range (Å)	13.60–2.00	13.43–2.00
R_{work}[b]/R_{free}[c]	0.1761/0.2139	0.1731/0.2098
Number of protein atoms	2839	17039
Number of water atoms	318	1883
RMSD[d] bond lengths (Å)	0.007	0.019
RMSD bond angles (°)	0.896	1.844
Average B-factors (Å^2)	21.7	24.0
Ramachandran plot[e] (residues, %)		
Most favored	95.87	96.04
Additional allowed	4.13	3.56
Outliers	0.00	0.40
Protein Data Bank entry	7DMN	7DMO

[a]$R_{merge} = \sum_{hkl}\sum_i|I_i(hkl) - \langle I(hkl)\rangle|/\sum_{hkl}\sum_i I_i(hkl)$, where $I_i(hkl)$ is the intensity of an

observation and <$I(hkl)$> is the mean value for its unique reflection. Summations are over all reflections.

[b]$R_{work} = \sum_h |F_o(h)-F_c(h)|/\sum_h F_o(h)$, where F_o and F_c are the observed and calculated structure factor amplitudes, respectively.

[c]R_{free} was calculated with 5% of the data excluded from the refinement.

[d]RMSD, root mean square deviation from ideal values.

[e]The categories were defined by Molprobity.

Figure S1. Natural pericyclases catalyzing [4 + 2] and [6 + 4] cycloaddition reactions in the biosynthesis of natural products. These biosynthetic pericyclases include Sol5 in solanapyrone B biosynthesis,[1] UcsH in UCS1025A biosynthesis,[2] PoxQ in oxaleimide A biosynthesis,[3] Bet1 in betaenone biosynthesis,[4] PvhB in varicidin B biosynthesis,[5] CghA in Sch210972 biosynthesis,[6] MycB in myceliothermophin B biosynthesis,[7] LovB in lovaststin biosynthesis,[8] IccD in ilicicolin biosynthesis,[9] ChaB in chaetolivacines B biosynthesis,[10] StmD in streptoseomycin biosynthesis,[11] NgnD in nargenicin biosynthesis,[11] Epil in fusaricide biosynthesis,[12] LepI in leporin C biosynthesis,[13,14] IdmH in indanomycin biosynthesis,[15] CrcS in catharanthine biosynthesis,[16] TitabS in tabersonine biosynthesis,[16] AbmU in neoabyssomicin B biosynthesis,[17] AbyU in abyssomicin C biosynthesis,[18] PhqE in Paraherquamide A biosynthesis,[19] MalC in malbrancheamide biosynthesis,[20] PyiF in pyrichalasin H biosynthesis, [3] CcsF in cytochalasin K biosynthesis,[21] VstJ in versipelostatin biosynthesis,[22] SpnF in spinosyn biosynthesis,[23] PyrE3 and PyrI4 in pyrroidomycin biosynthesis,[24] TbtD in thiomuracin GZ biosynthesis,[25] TclM in thiocillins biosynthesis,[26] PbtD in GE2270A biosynthesis,[27] EupfF in neosetophomone B biosynthesis,[28] SorD in spirosorbicillinol B biosynthesis,[29] MaDA in chalcomoracin biosynthesis,[30] AsR5 in xenovulene A biosynthesis,[31] riboflavin synthase in riboflavin biosynthesis.[32]

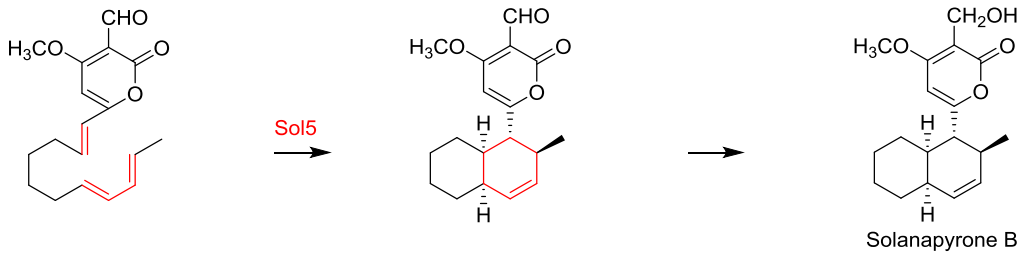
Sol5
Solanapyrone B

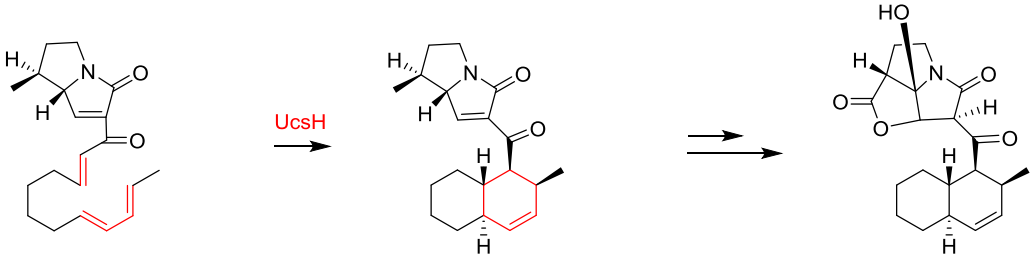
UcsH
UCS1025A

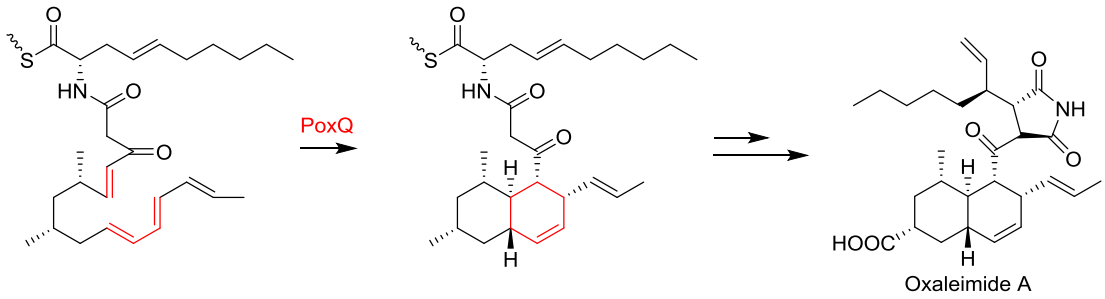
PoxQ
Oxaleimide A

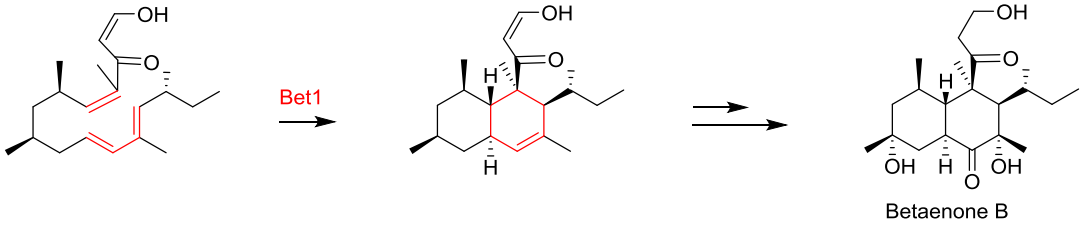
Bet1
Betaenone B

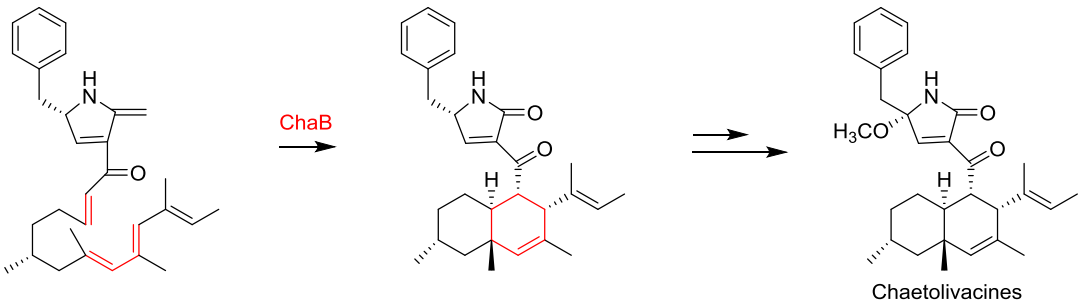
ChaB
Chaetolivacines

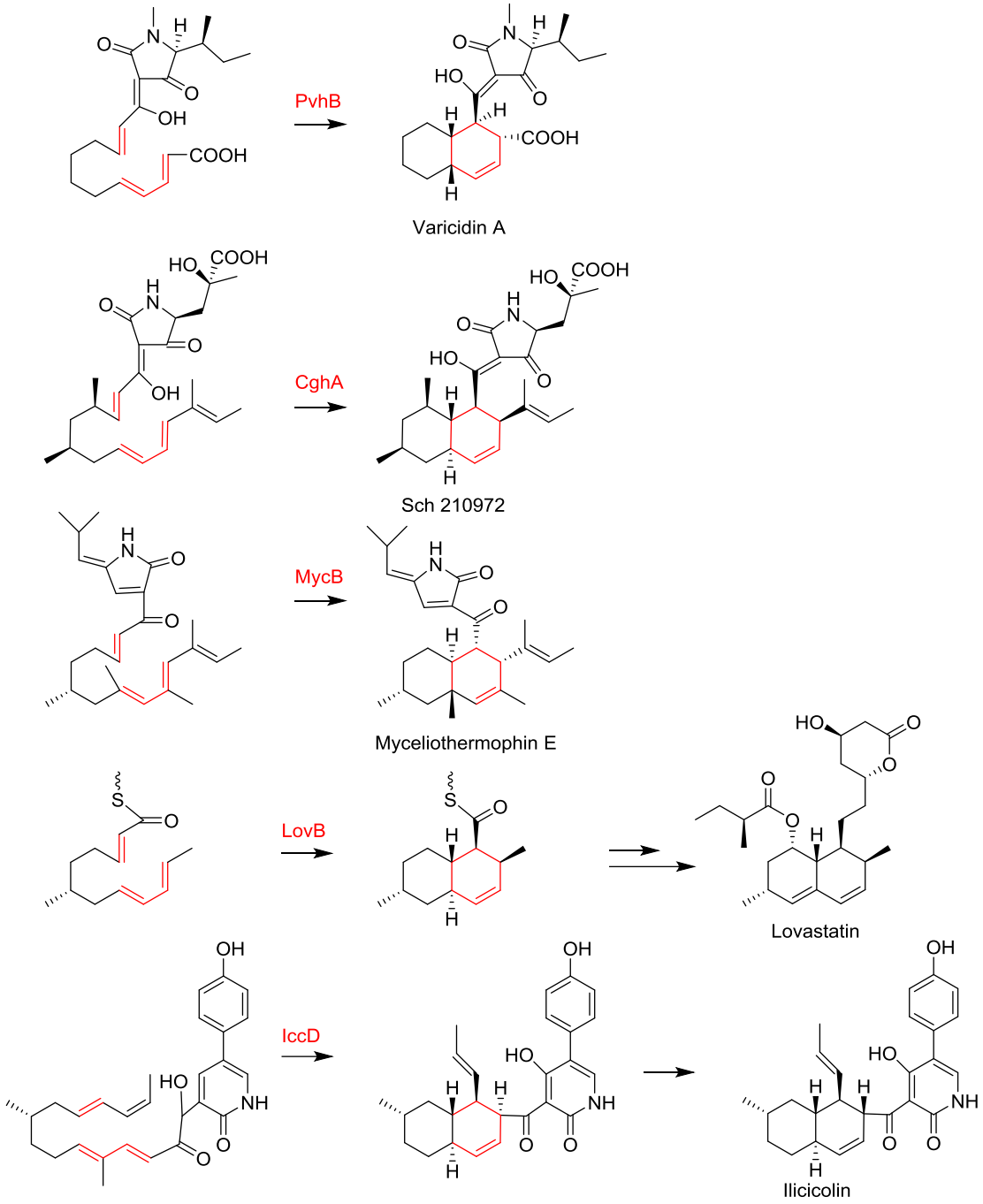
PvhB
Varicidin A
CghA
Sch 210972
MycB
Myceliothermophin E
LovB
Lovastatin
IccD
Ilicicolin

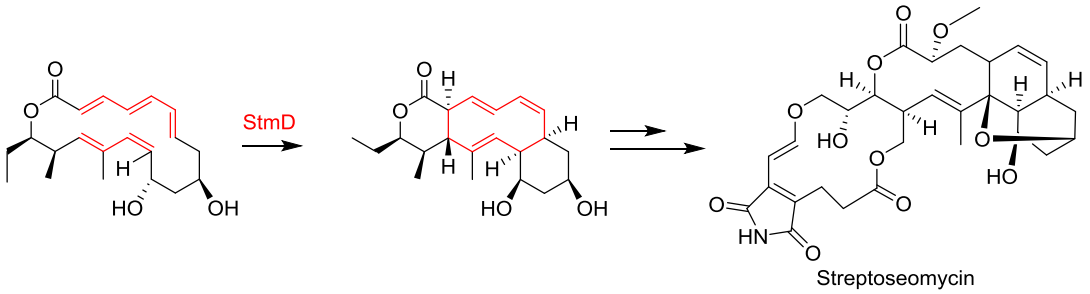
StmD
Streptoseomycin

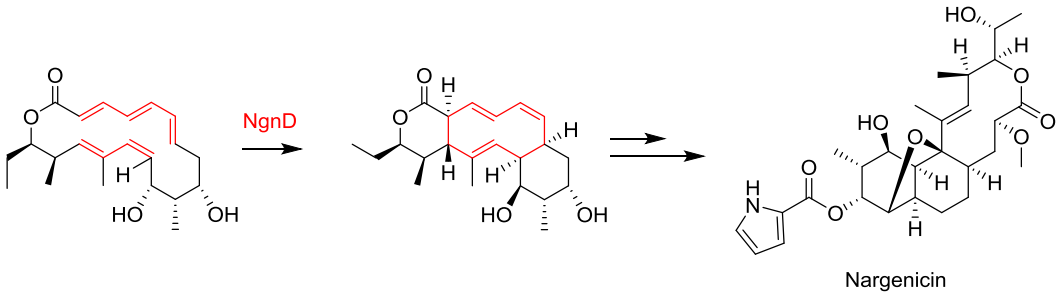
NgnD
Nargenicin

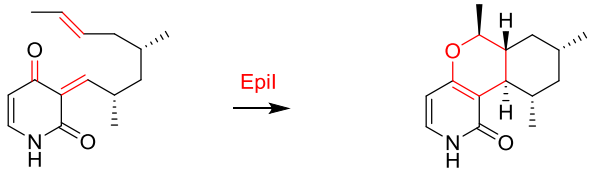
EpiI

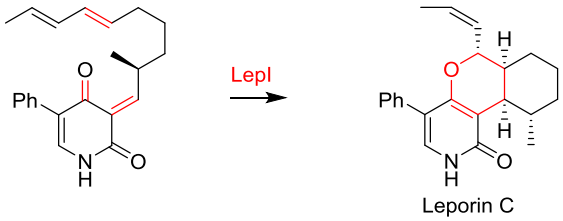
LepI
Leporin C

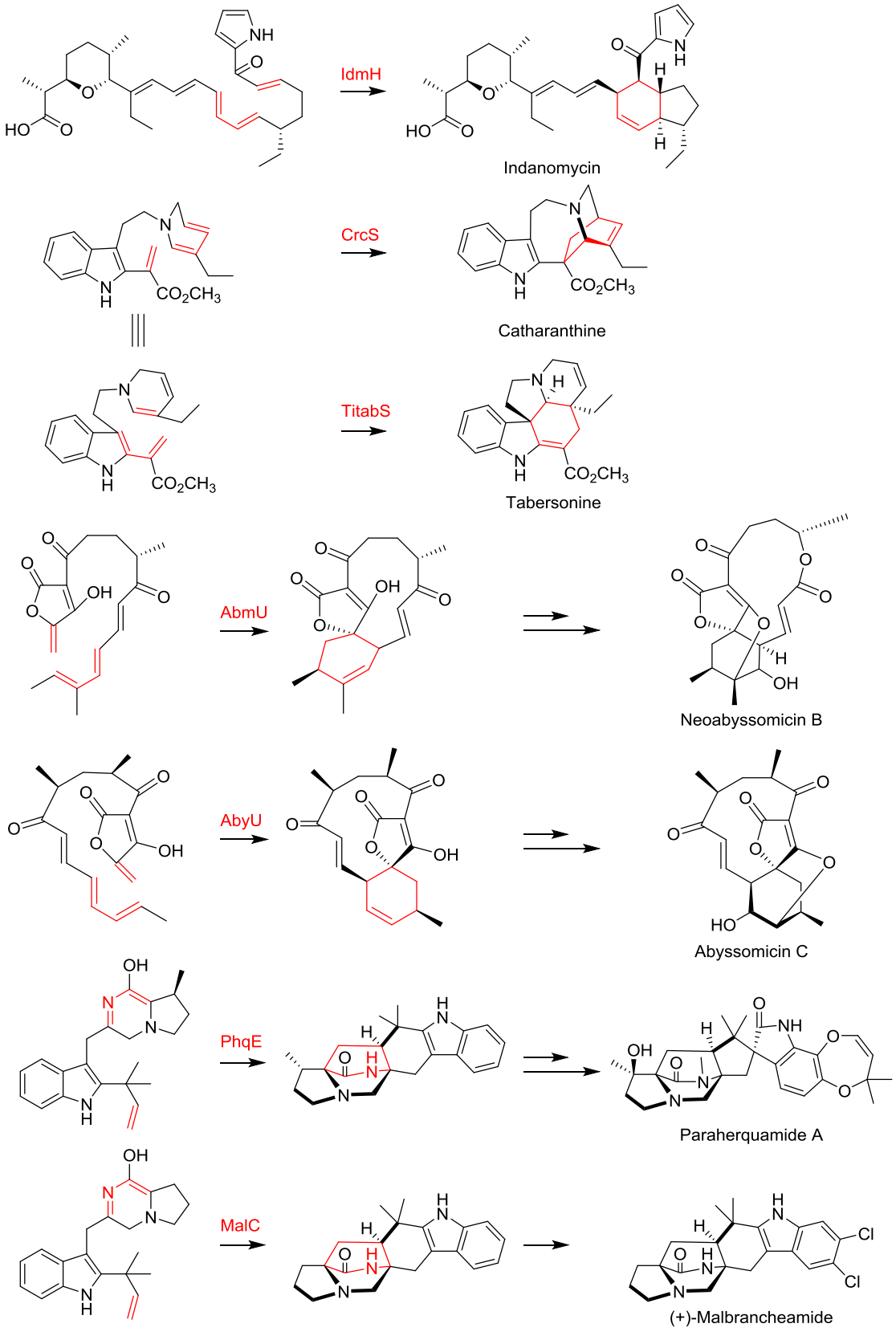
IdmH
Indanomycin
CrcS
Catharanthine
TitabS
Tabersonine
AbmU
Neoabyssomicin B
AbyU
Abyssomicin C
PhqE
Paraherquamide A
MalC
(+)-Malbrancheamide

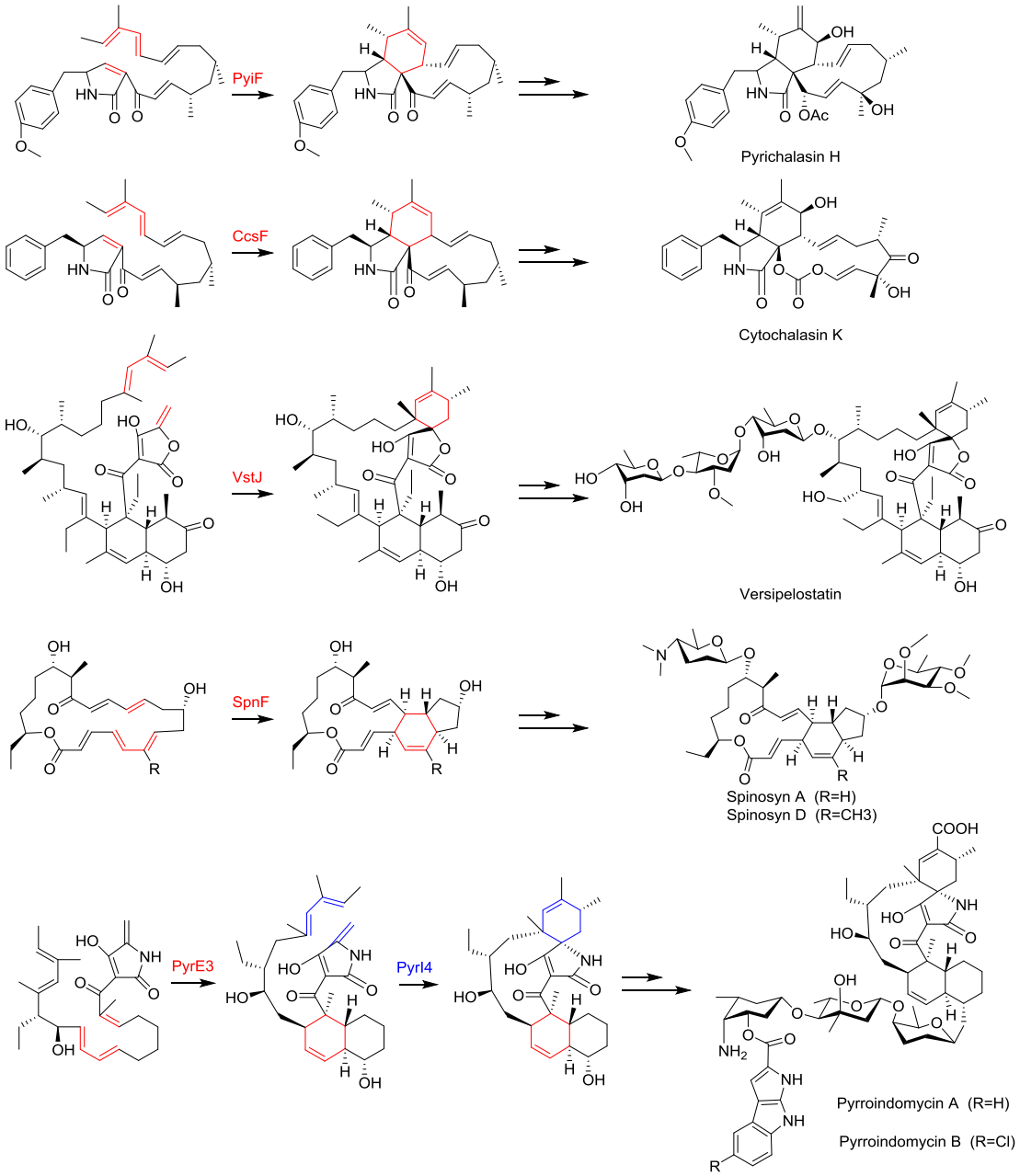
PyiF
Pyrichalasin H
CcsF
Cytochalasin K
VstJ
Versipelostatin
SpnF
Spinosyn A (R=H)
Spinosyn D (R=CH3)
PyrE3
PyrI4
Pyrroindomycin A (R=H)
Pyrroindomycin B (R=Cl)

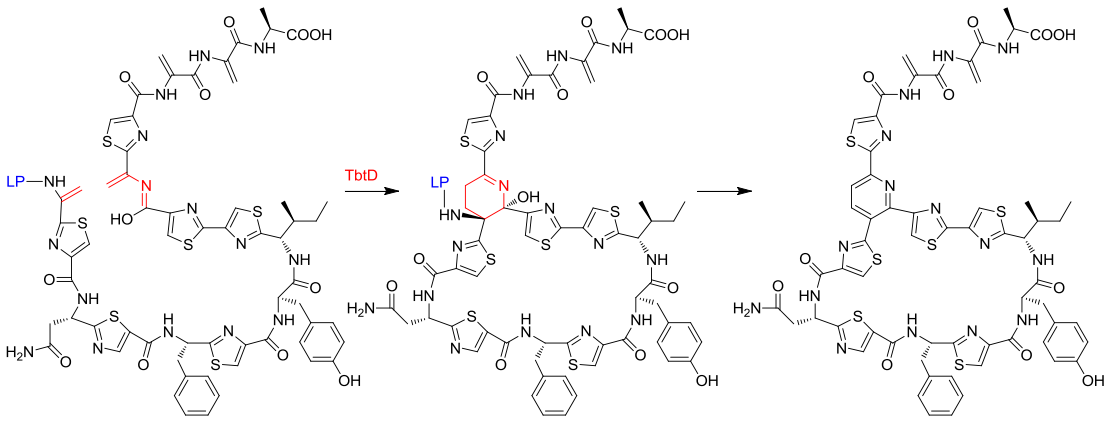
TbtD
LP
Thiomuracin GZ

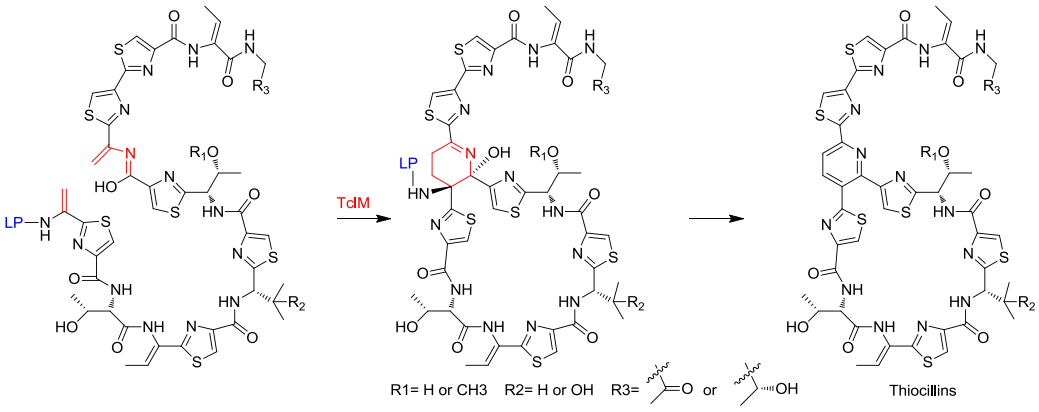
TclM
LP
R1= H or CH3
R2= H or OH
R3=
or
Thiocillins

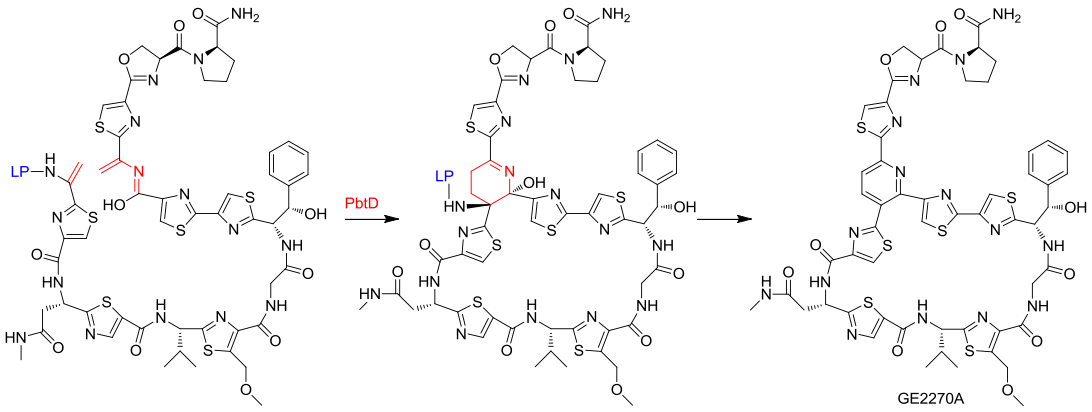
PbtD
LP
GE2270A

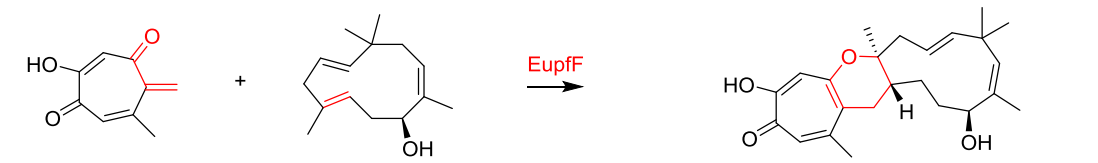
EupfF
Neosetophomone B

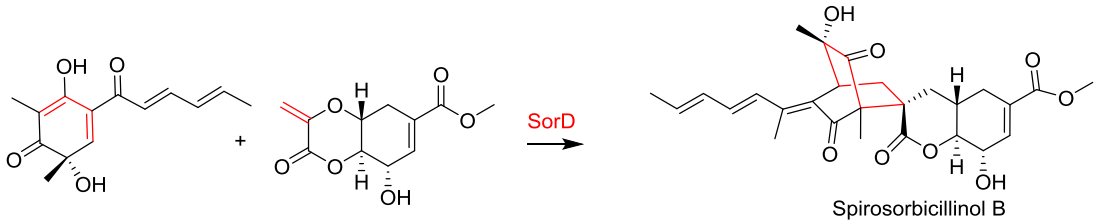
SorD
Spirosorbicillinol B

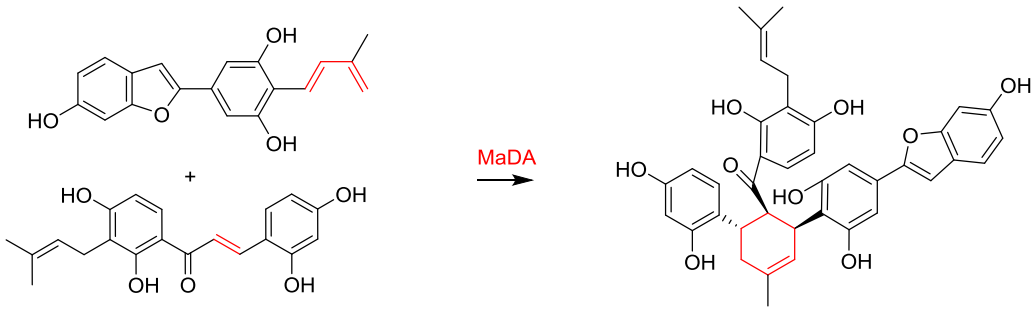
MaDA
Chalcomoracin

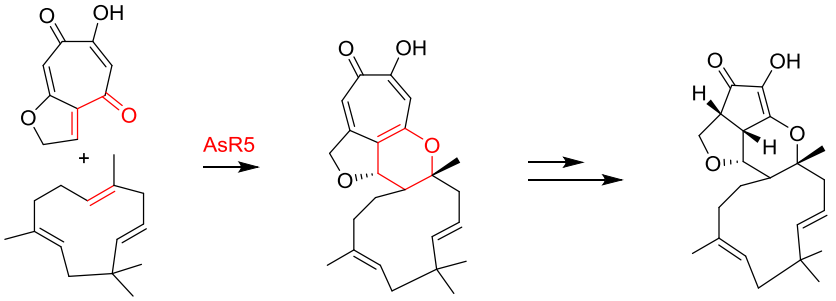
AsR5
Xenovulene A

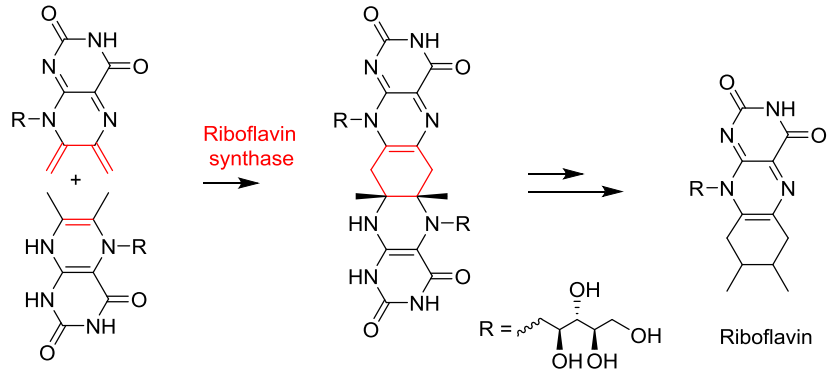
Riboflavin synthase
Riboflavin

Figure S2. The SDS-PAGE analysis of purified Se-Fsa2 and Phm7.

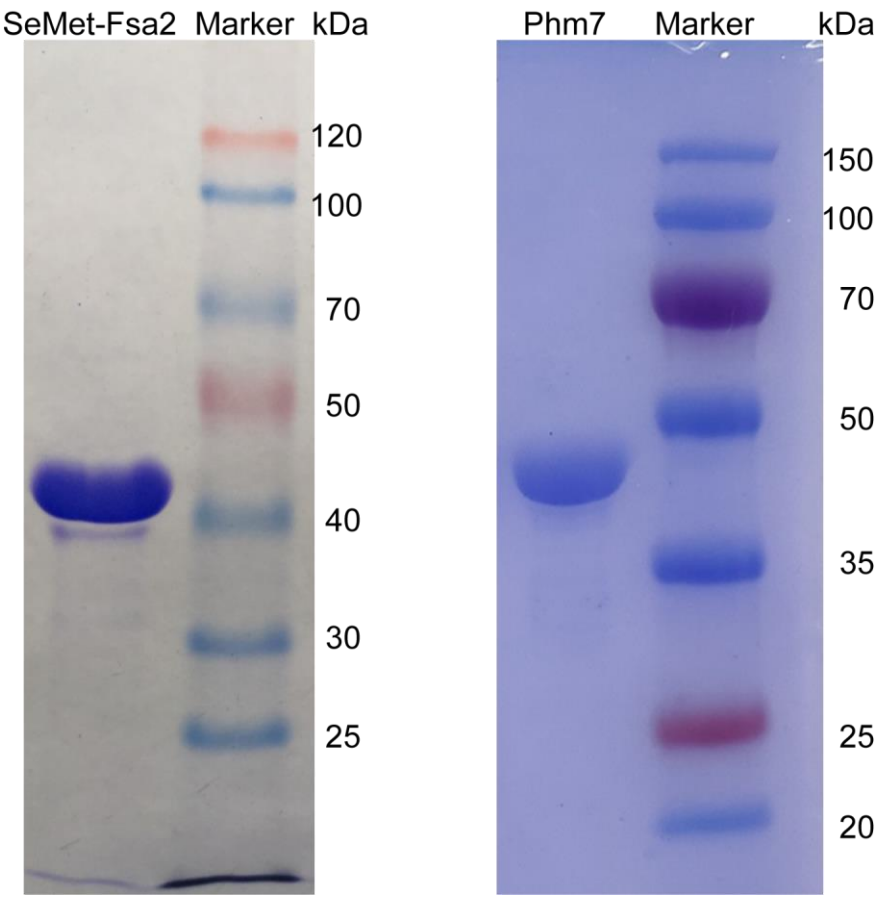

Figure S3. The β barrels in Fsa2 and Phm7. (A) The two β barrels in Fsa2 are orthogonally packed with each axis perpendicular to the other. (B) The two β barrels in Phm7 are orthogonally packed with each axis perpendicular to the other. (C) The long loop (green) between β1 and β2 covers one side of entrance of the N-terminal β barrel in Fsa2, and this loop interacts with another long loop (blue) between β10 and β11. (D) The long loop (green) between β1 and β2 covers one side of entrance of the N-terminal β barrel in Phm7, and this loop interacts with another long loop (blue) between β10 and β11.

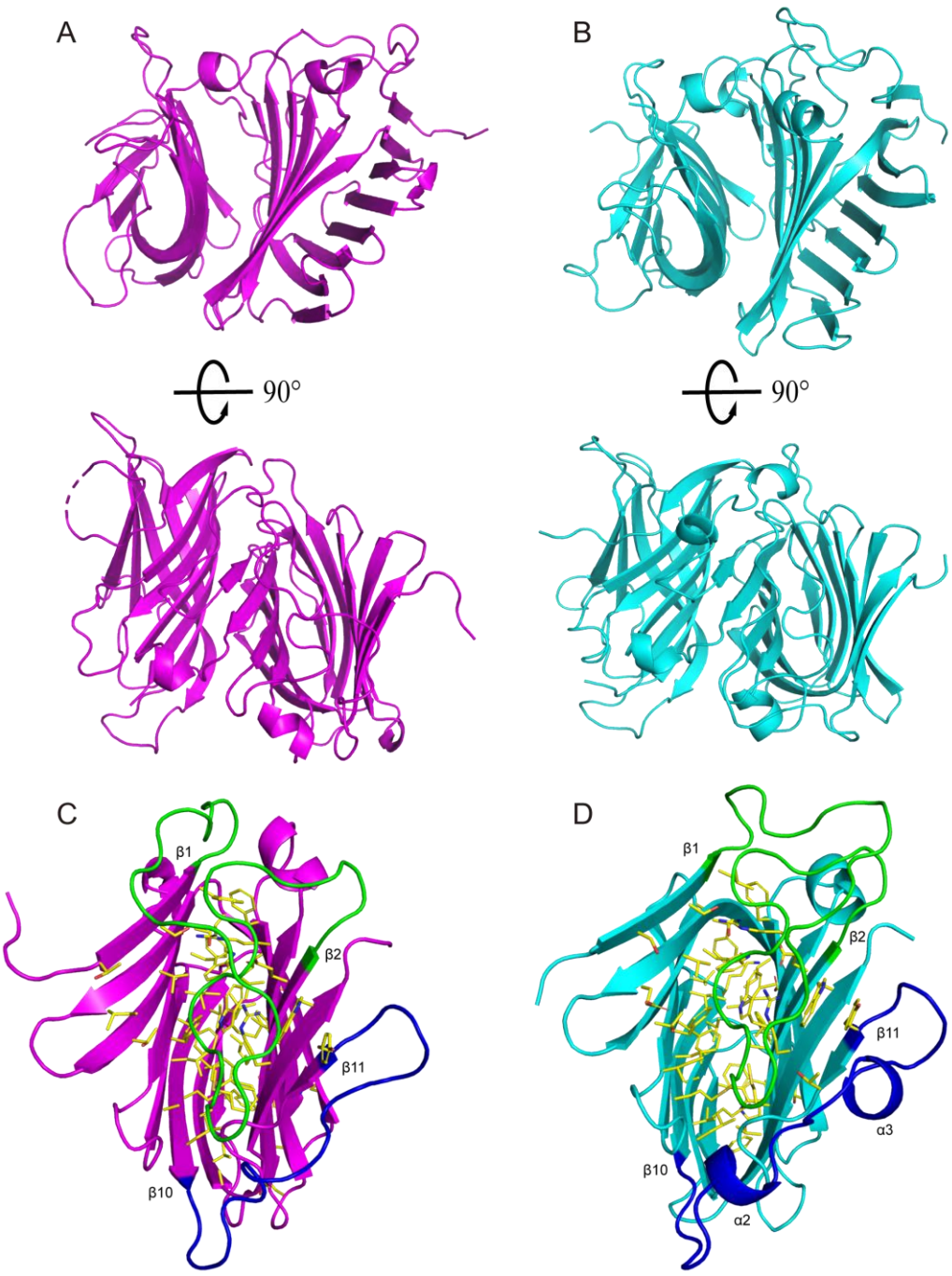

Figure S4. Structural superimposition of N- and C-terminal β barrels in Fsa2 or Phm7. (A) Structural superimposition of N- and C-terminal β barrels in Fsa2 gives a RMSD of 3.37 Å for 108 Cα atoms. (B) Structural superimposition of N- and C-terminal β barrels in Phm7 gives a RMSD of 3.37 Å for 108 Cα atoms.

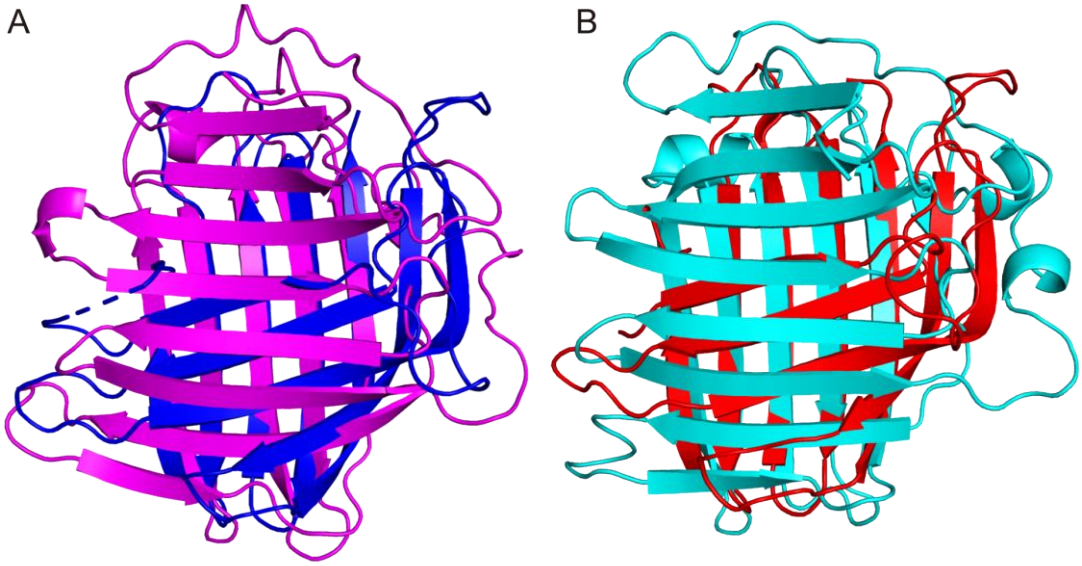

Figure S5. The six molecules in one asymmetric unit of Phm7. (A) The six molecules of Phm7 are shown in green, cyan, yellow, orange, red and pink in one asymmetric unit. (B) Superimposition of the six molecules in one asymmetric unit of Phm7 shows that their tertiary structures are almost the same. Colors were shown as the same to those in (A).

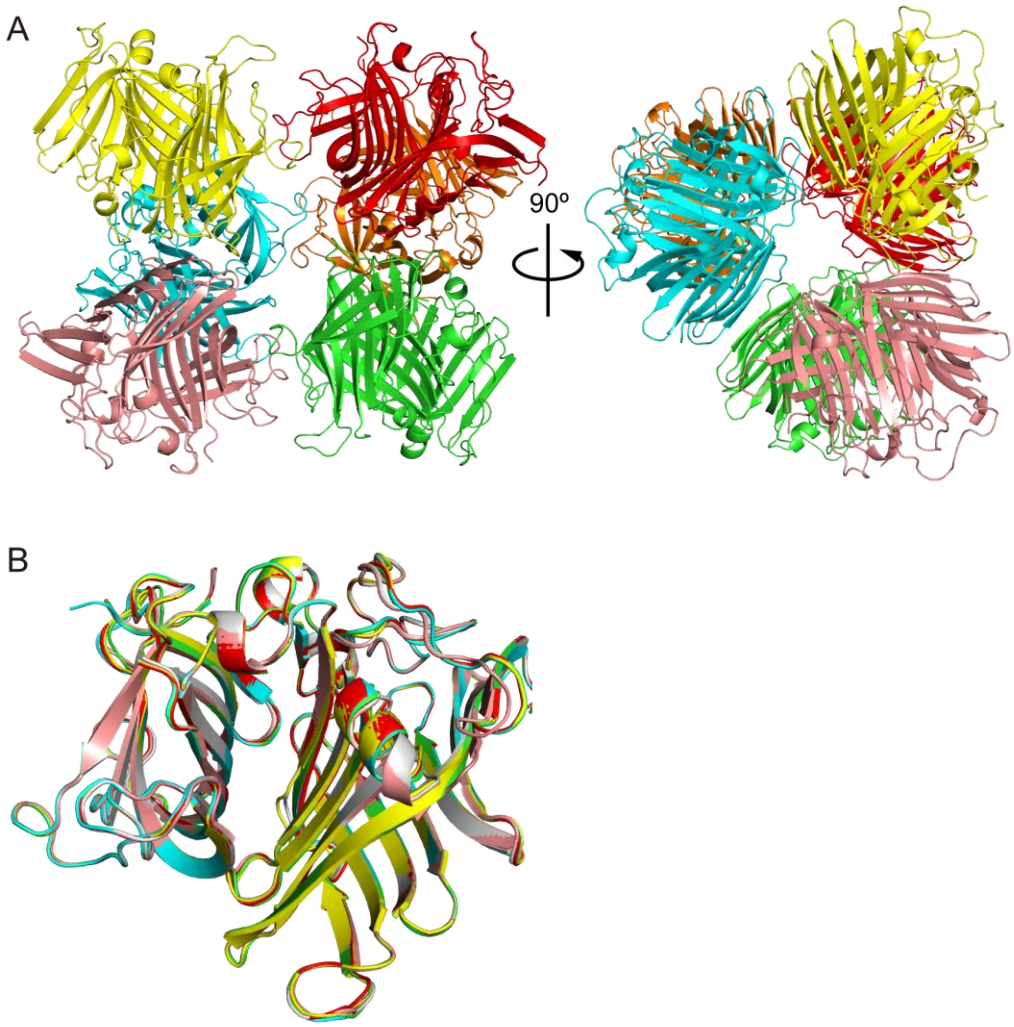

Figure S6. Sequence alignment of Fsa2, Phm7, and CghA. Secondary structure elements of Fsa2 and Phm7 are shown at the top and the bottom, respectively. The sequences of Fsa2, CghA and Phm7 are from the following organisms: *Fusarium* sp. FN080326 (Fsa2, A0A0E4AYE7.1), *Chaetomium globosum* strain ATCC 6205 (CghA, EAQ90433.1), *Pyrenochaetopsis* sp. (Phm7, BBC43190.1).

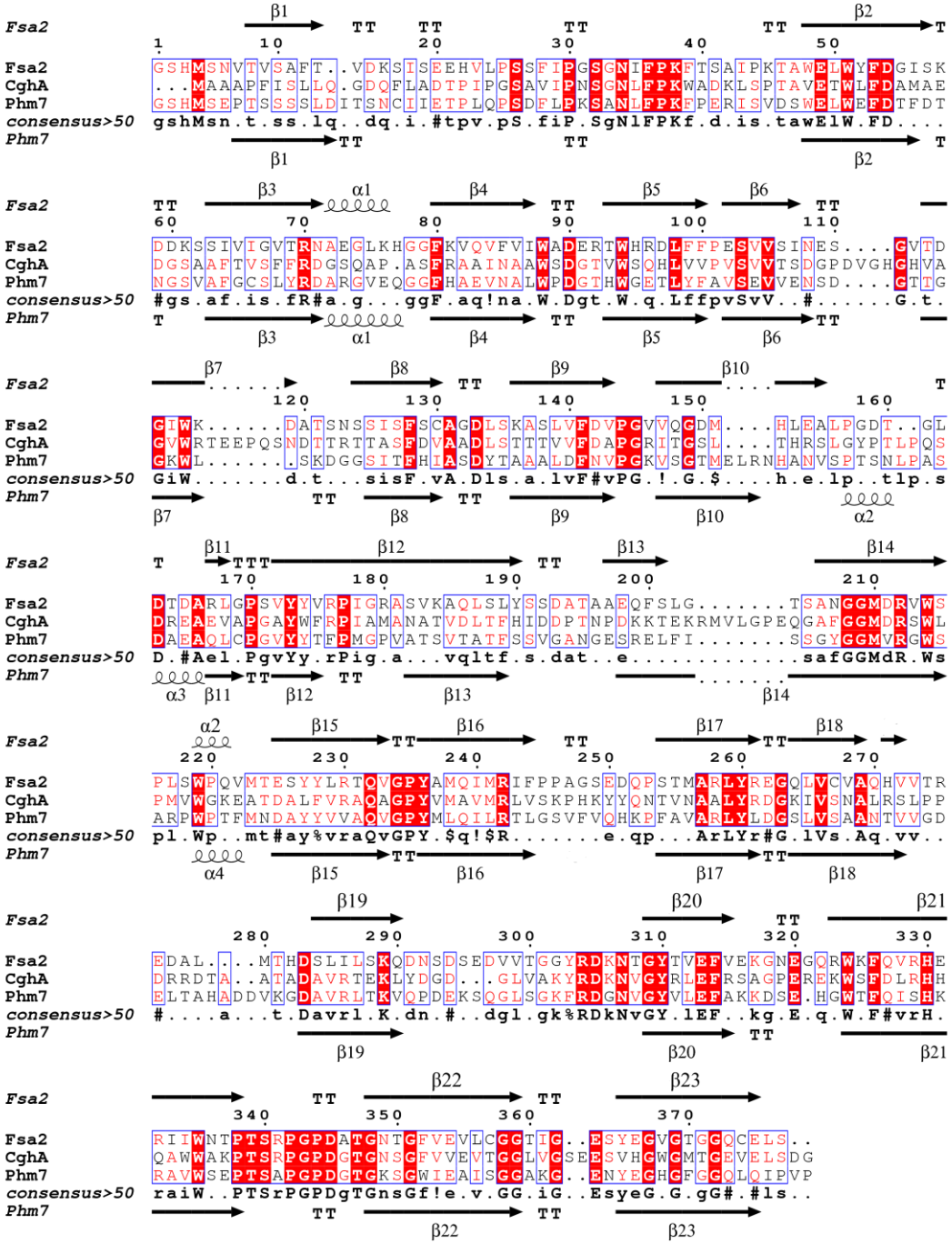

Figure S7. Structural comparisons of N- and C-terminal β barrels of Fsa2 with PyrI4, AbyU, and AbmU. (A) Superimposition of N-terminal β barrel (magenta) of Fsa2 with PyrI4 (green, PDB ID: 5BU3). (B) Superimposition of N-terminal β barrel (magenta) of Fsa2 with AbyU (yellow, PDB ID: 5DYV). (C) Superimposition of N-terminal β barrel (magenta) of Fsa2 with AbmU (blue, PDB ID: 6LE0). (D) Superimposition of C-terminal β barrel (magenta) of Fsa2 with PyrI4 (green). (E) Superimposition of C-terminal β barrel (magenta) of Fsa2 with AbyU (yellow). (F) Superimposition of C-terminal β barrel (magenta) of Fsa2 with AbmU (blue). All these comparisons show that the N- and C-terminal β barrels of Fsa2 are much more flattened than those of PyrI4, AbyU, and AbmU. Similar results were observed for structural comparisons of N- and C-terminal β barrels of Phm7 with PyrI4, AbyU, and AbmU.

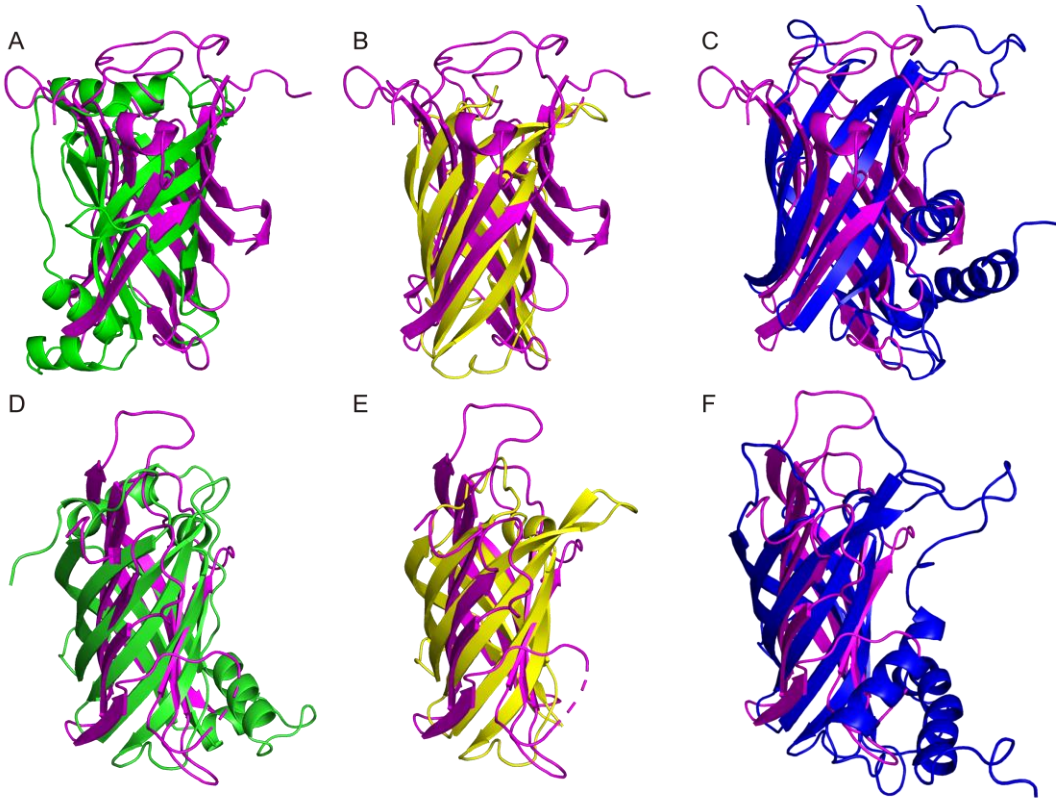

Figure S8. The two glycerol molecules in the active site of Fsa2 and their interactions with Ser226. (A) The two glycerol molecules (green sticks) in the active site of Fsa2. (B) Ser226 interacts with two water molecules (red spheres), which forms hydrogen bonds (yellow dashed lines) with the two glycerol molecules in Fsa2 structures.

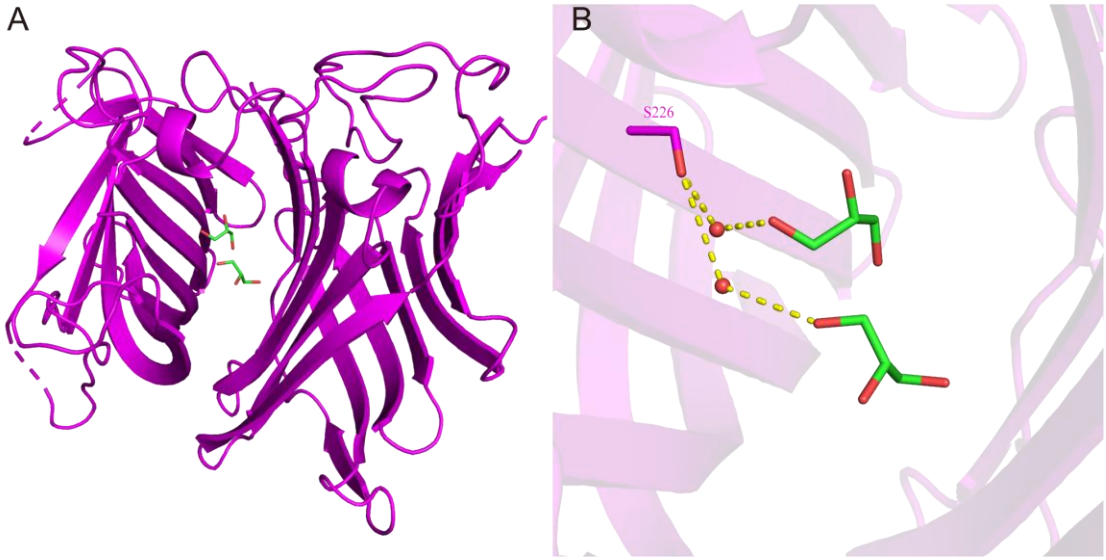

Figure S9. The products modeling into the active sites of Fsa2 and Phm7. (A) Modeling of **7** (green) in the active site of Fsa2. (B) Modeling of **6** (yellow) in the active site of Phm7. Residues' names are labelled in magenta for Fsa2 and blue for Phm7. The hydrogen bonds are indicated with yellow dashed lines.

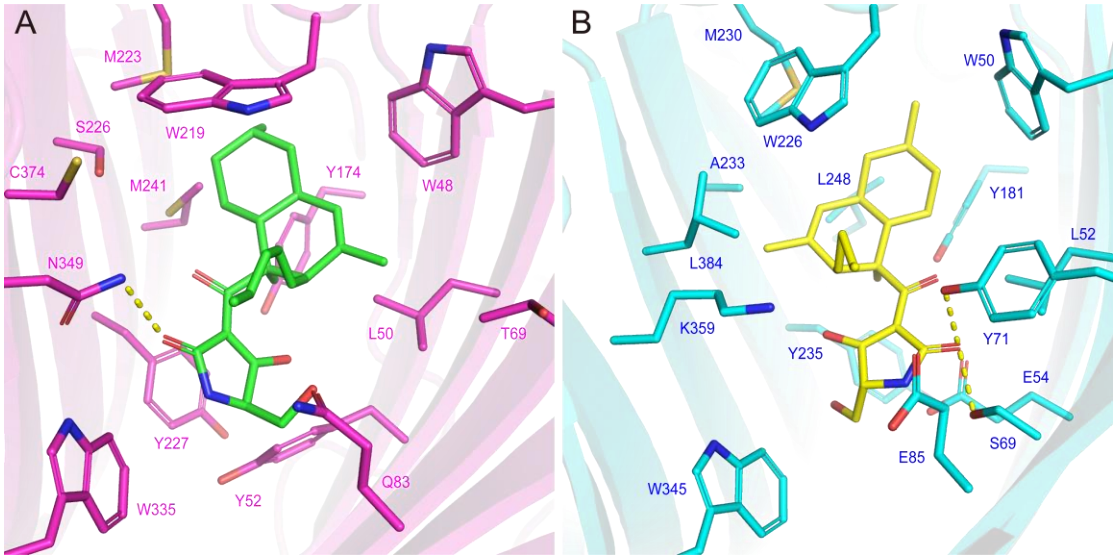

Figure S10. Comparison of the modeled **6** within the active site of Phm7 and the complex structure of CghA with its product Sch210972. (A) Active sites comparison of Phm7 (cyan) and CghA (orange). Residues' names are labelled in cyan for Phm7 and blue for CghA. (B) The complex structure of CghA with its product Sch210972. Sch210972 is shown in grey sticks, and hydrogen bonds are shown with yellow dashed line. (C) Superimposition of the modeled **6** (yellow sticks) within the active site of Phm7 and Sch210972 (grey sticks) in the complex structure of CghA.

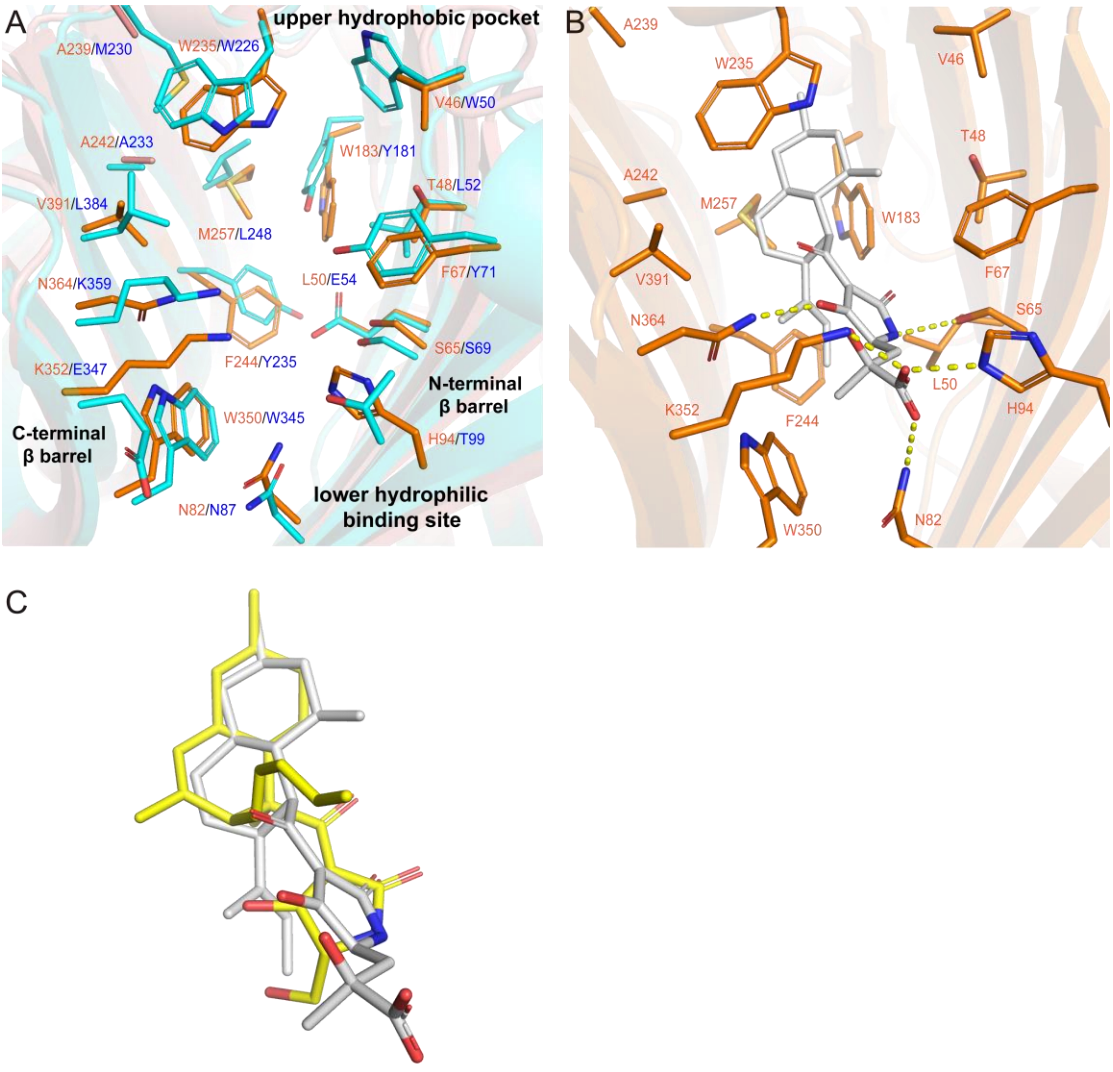

Figure S11. The molecular dynamics simulation of **5**-bound Fsa2. (A) The molecular dynamics simulation of **5**-bound Fsa2 (**5** in cyan and Fsa2 in gray). The hydrogen bonds are indicated with yellow dashed lines. (B) Structural superimposition of **5**-bound Fsa2 between molecular dynamics simulation (**5** in cyan and Fsa2 in gray) and substrate modeling (**5** in green and Fsa2 in magenta).

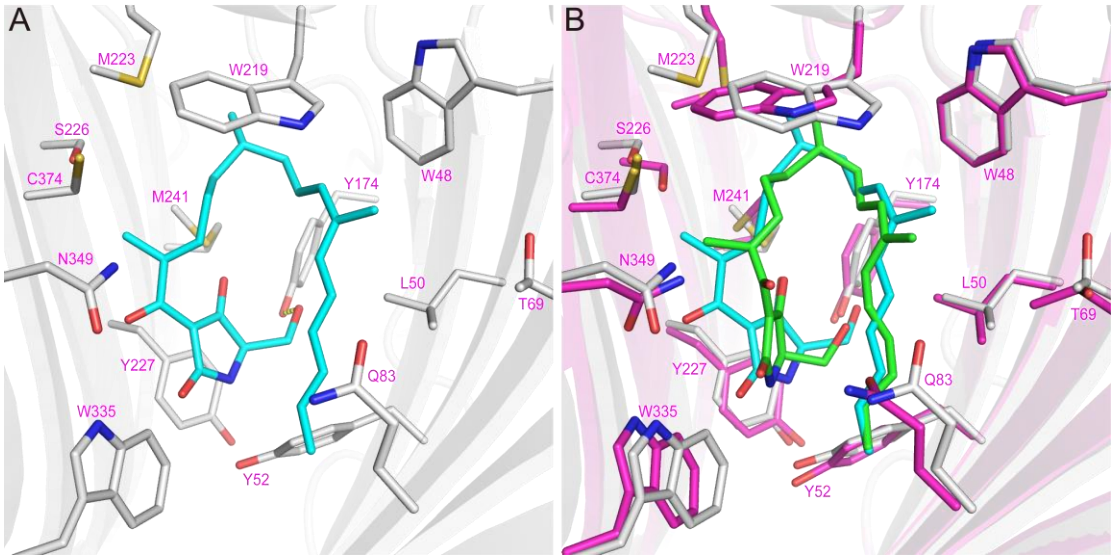

Figure S12. The molecular dynamics simulation of **5**-bound Phm7. (A) The molecular dynamics simulation of **5**-bound Phm7 (**5** in magenta and Phm7 in gray). The hydrogen bonds are indicated with yellow dashed lines. (B) Structural superimposition of **5**-bound Phm7 between molecular dynamics simulation (**5** in magenta and Phm7 in gray) and substrate modeling (**5** in yellow and Phm7 in cyan).

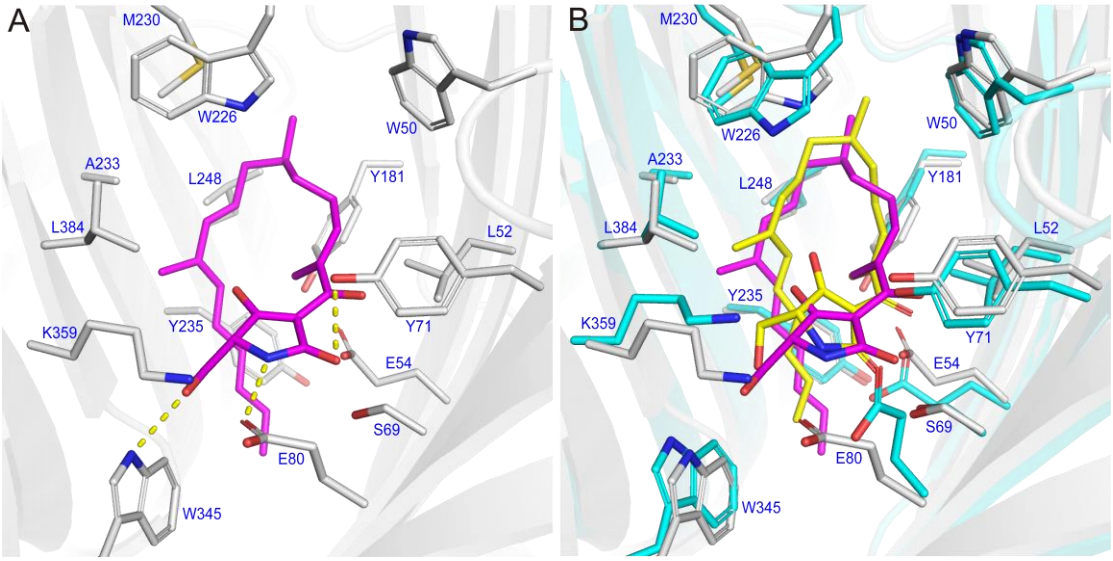

Reference

(1) Kasahara, K.; Miyamoto, T.; Fujimoto, T.; Oguri, H.; Tokiwano, T.; Oikawa, H.; Ebizuka, Y.; Fujii, I. Solanapyrone Synthase, a Possible Diels-Alderase and Iterative Type I Polyketide Synthase Encoded in a Biosynthetic Gene Cluster from *Alternaria Solani*. *ChemBioChem.* **2010**, *11*, 1245–1252.

(2) Li, L.; Tang, M. C.; Tang, S.; Gao, S.; Soliman, S.; Hang, L.; Xu, W.; Ye, T.; Watanabe, K.; Tang, Y. Genome Mining and Assembly-Line Biosynthesis of the UCS1025A Pyrrolizidinone Family of Fungal Alkaloids. *J. Am. Chem. Soc.* **2018**, *140*, 2067–2071.

(3) Hantke, V.; Skellam, E. J.; Cox, R. J. Evidence for Enzyme Catalysed Intramolecular [4 + 2] Diels-Alder Cyclization during the Biosynthesis of Pyrichalasin H. *Chem. Commun.* **2020**, *56*, 2925–2928.

(4) Ugai, T.; Minami, A.; Fujii, R.; Tanaka, M.; Oguri, H.; Gomi, K.; Oikawa, H. Heterologous Expression of Highly Reducing Polyketide Synthase Involved in Betaenone Biosynthesis. *Chem. Commun.* **2015**, *51*, 1878–1881.

(5) Tan, D.; Jamieson, C. S.; Ohashi, M.; Tang, M.; Houk, K. N.; Tang, Y. Genome-Mined Diels − Alderase Catalyzes Formation of the *cis*-Octahydrodecalins of Varicidin A and B. *J. Am. Chem. Soc.* **2019**,*141*, 4–8.

(6) Sato, M.; Yagishita, F.; Mino, T.; Uchiyama, N.; Patel, A.; Chooi, Y. H.; Goda, Y.; Xu, W.; Noguchi, H.; Yamamoto, T.; Hotta, K.; Houk, K. N.; Tang, Y.; Watanabe, K. Involvement of Lipocalin-like CghA in Decalin-Forming Stereoselective Intramolecular [4+2] Cycloaddition. *ChemBioChem.* **2015**, *16*, 2294–2298.

(7) Li, L.; Yu, P.; Tang, M. C.; Zou, Y.; Gao, S. S.; Hung, Y. S.; Zhao, M.; Watanabe, K.; Houk, K. N.; Tang, Y. Biochemical Characterization of a Eukaryotic Decalin-Forming Diels-Alderase. *J. Am. Chem. Soc.* **2016**, *138*, 15837–15840.

(8) Auclair, K.; Sutherland, A.; Kennedy, J.; Witter, D. J.; Van Den Heever, J. P.; Hutchinson, C. R.; et al. Lovastatin Nonaketide Synthase Catalyzes an Intramolecular Diels-Alder Reaction of a Substrate Analogue. *J. Am. Chem. Soc.* **2000**, *122*, 11519-11520.

(9) Zhang, Z.; Jamieson, C. S.; Zhao, Y. L.; Li, D.; Ohashi, M.; Houk, K. N.; Tang, Y. Enzyme-Catalyzed Inverse-Electron Demand Diels-Alder Reaction in the Biosynthesis of Antifungal Ilicicolin H. *J. Am. Chem. Soc.* **2019**, *141*, 5659–5663.

(10) Wang, X.; Zhao, L.; Liu, C.; Qi, J.; Zhao, P.; Liu, Z.; Li, C. New Tetramic Acids Comprising of Decalin and Pyridones From *Chaetomium Olivaceum* SD-80A With Antimicrobial Activity. *Front Microbiol.* **2020**, *10*, 1–11.

(11) Zhang, B.; Wang, K. B.; Wang, W.; Wang, X.; Liu, F.; Zhu, J.; Shi, J.; Li, L. Y.; Han, H.; Xu, K.; Qiao, H. Y.; Zhang, X.; Jiao, R. H.; Houk, K. N.; Liang, Y.; Tan, R. X.; Ge, H. M. Enzyme-Catalysed [6+4] Cycloadditions in the Biosynthesis of Natural Products. *Nature.* **2019**, *568*, 122–126.

(12) Ohashi, M.; Jamieson, C. S.; Cai, Y.; Tan, D.; Kanayama, D.; Tang, M. C.; Anthony, S. M.; Chari, J. V.; Barber, J. S.; Picazo, E.; Kakule, T. B.; Cao, S.; Garg, N. K.; Zhou, J.; Houk, K. N.; Tang, Y. An Enzymatic Alder-Ene Reaction. *Nature.* **2020**, *586*, 64–69.

(13) Cai, Y.; Hai, Y.; Ohashi, M.; Jamieson, C. S.; Garcia-Borras, M.; Houk, K. N.; Zhou, J.; Tang, Y. Structural Basis for Stereoselective Dehydration and Hydrogen-Bonding Catalysis by the SAM-Dependent Pericyclase LepI. *Nat. Chem.* **2019**, *11*, 812–820.

(14) Ohashi, M.; Liu, F.; Hai, Y.; Chen, M.; Tang, M. cheng; Yang, Z.; Sato, M.; Watanabe, K.; Houk, K. N.; Tang, Y. SAM-Dependent Enzyme-Catalysed Pericyclic Reactions in Natural Product Biosynthesis. *Nature.* **2017**, *549*, 502–506.

(15) Drulyte, I.; Obajdin, J.; Trinh, C. H.; Kalverda, A. P.; Van Der Kamp, M. W.; Hemsworth, G. R.; Berry, A. Crystal Structure of the Putative Cyclase IdmH from the Indanomycin Nonribosomal Peptide Synthase/Polyketide Synthase. *IUCrJ.* **2019**, *6*, 1120–1133.

(16) Farrow, S. C.; Kamileen, M. O.; Caputi, L.; Bussey, K.; Mundy, J. E. A.; McAtee, R. C.; Stephenson, C. R. J.; O'Connor, S. E. Biosynthesis of an Anti-Addiction Agent from the Iboga Plant. *J. Am. Chem. Soc.* **2019**, *141*, 12979–12983.

(17) Li, Q.; Ding, W.; Tu, J.; Chi, C.; Huang, H.; Ji, X.; Yao, Z.; Ma, M.; Ju, J. Nonspecific Heme-Binding Cyclase, AbmU, Catalyzes [4+2] Cycloaddition during Neoabyssomicin Biosynthesis. *ACS. Omega.* **2020**, *5*, 20548–20557.

(18) Byrne, M. J.; Lees, N. R.; Han, L. C.; Van Der Kamp, M. W.; Mulholland, A. J.; Stach, J. E. M.; Willis, C. L.; Race, P. R. The Catalytic Mechanism of a Natural Diels-Alderase Revealed in Molecular Detail. *J. Am. Chem. Soc.* **2016**, *138*, 6095–6098.

(19) Fraley, A. E.; Caddell Haatveit, K.; Ye, Y.; Kelly, S. P.; Newmister, S. A.; Yu, F.; Williams, R. M.; Smith, J. L.; Houk, K. N.; Sherman, D. H. Molecular Basis for Spirocycle Formation in the Paraherquamide Biosynthetic Pathway. *J. Am. Chem. Soc.* **2020**, *142*, 2244–2252.

(20) Dan, Q. Y; Newmister, S. A.; Klas, K. R.; Fraley, A. E.; Timothy, J.; Somoza, A. D.; Sunderhaus, J. D.; Ye, Y.; Shende, V. V; Yu, F.; Sanders, J. N.; Brown, W. C.; Zhao, L.; Paton, R. S.; Houk, K. N.; Smith, J. L.; Sherman, D. H.; Williams, R. M. Fungal Indole Alkaloid Biogenesis Through Evolution of a Bifunctional Reductase/Diels-Alderase. *Nat. Chem.* **2020**, *11*, 972– 980.

(21) Fujii, R.; Minami, A.; Gomi, K.; Oikawa, H. Biosynthetic Assembly of Cytochalasin Backbone. *Tetrahedron Lett.* **2013**, *54*, 2999–3002.

(22) Hashimoto, T.; Hashimoto, J.; Teruya, K.; Hirano, T.; Shin-Ya, K.; Ikeda, H.; Liu, H. W.; Nishiyama, M.; Kuzuyama, T. Biosynthesis of Versipelostatin: Identification of an Enzyme-Catalyzed [4+2]-Cycloaddition Required for Macrocyclization of Spirotetronate-Containing Polyketides. *J. Am. Chem. Soc.* **2015**, *137*, 572–575.

(23) Yang, G.; Sau, C.; Lai, W.; Cichon, J.; Li, W. The Structure of SpnF, a Standalone Enzyme That Catalyzes [4+2] Cycloaddition. *Nat. Chem. Biol.* **2015**, *344*, 1173–1178.

(24) Tian, Z.; Sun, P.; Yan, Y.; Wu, Z.; Zheng, Q.; Zhou, S.; Zhang, H.; Yu, F.; Jia, X.; Chen, D.; Mándi, A.; Kurtán, T.; Liu, W. An Enzymatic [4+2] Cyclization Cascade Creates the Pentacyclic Core of Pyrroindomycins. *Nat. Chem. Biol.* **2015**, *11*, 259–265.

(25) Bogart, J. W.; Bowers, A. A. Thiopeptide Pyridine Synthase TbtD Catalyzes an Intermolecular Formal Aza-Diels-Alder Reaction. *J. Am. Chem. Soc.* **2019**, *141*, 1842–1846.

(26) Wever, W. J.; Bogart, J. W.; Baccile, J. A.; Chan, A. N.; Schroeder, F. C.; Bowers, A. A. Chemoenzymatic Synthesis of Thiazolyl Peptide Natural Products Featuring an Enzyme-Catalyzed Formal [4+2] Cycloaddition. *J. Am. Chem. Soc.* **2015**, *137*, 3494–3497.

(27) Cogan, D. P.; Hudson, G. A.; Zhang, Z.; Pogorelov, T. V.; Van Der Donk, W. A.; Mitchell, D. A.; Nair, S. K. Structural Insights into Enzymatic [4+2] Aza-Cycloaddition in Thiopeptide Antibiotic Biosynthesis. *Proc. Natl. Acad. Sci. U. S. A.* **2017**, *114*, 12928–12933.

(28) Chen, Q.; Gao, J.; Jamieson, C.; Liu, J.; Ohashi, M.; Bai, J.; Yan, D.; Liu, B.; Che, Y.; Wang, Y.; Houk, K. N.; Hu, Y. Enzymatic Intermolecular Hetero-Diels-Alder Reaction in the Biosynthesis of Tropolonic Sesquiterpenes. *J. Am. Chem. Soc.* **2019**, *141*, 14052–14056.

(29) Kahlert, L.; Bassiony, E. F.; Cox, R. J.; Skellam, E. J. Diels–Alder Reactions During the Biosynthesis of Sorbicillinoids. *Angew. Chem. Int. Ed.* **2020**, *59*, 5816–5822.

(30) Gao, L.; Su, C.; Du, X.; Wang, R.; Chen, S.; Zhou, Y.; Liu, C.; Liu, X.; Tian, R.; Zhang, L.; Xie, K.; Chen, S.; Guo, Q.; Guo, L.; Hano, Y.; Shimazaki, M.; Minami, A.; Oikawa, H.; Huang, N.; Houk,

K. N.; Huang, L.; Dai, J.; Lei, X. FAD-Dependent Enzyme-Catalysed Intermolecular [4+2] Cycloaddition in Natural Product Biosynthesis. *Nat. Chem.* **2020**, *12*, 620–628.

(31) Schotte, C.; Li, L.; Wibberg, D.; Kalinowski, J.; Cox, R. J. Synthetic Biology Driven Biosynthesis of Unnatural Tropolone Sesquiterpenoids. *Angew. Chem. Int. Ed.* **2020**, 2–11.

(32) Kim, R. R.; Illarionov, B.; Joshi, M.; Cushman, M.; Lee, C. Y.; Eisenreich, W.; Fischer, M.; Bacher, A. Mechanistic Insights on Riboflavin Synthase Inspired by Selective Binding of the 6,7-Dimethyl-8-Ribityllumazine Exomethylene Anion. *J. Am. Chem. Soc.* **2010**, *132*, 2983–2990.